

# On-set of EHD turbulence for cylinder in cross flow under corona discharges

J.S. Chang<sup>a,\*</sup>, D. Brocilo<sup>a</sup>, K. Urashima<sup>a</sup>, J. Dekowski<sup>b</sup>, J. Podlinski<sup>b</sup>,  
J. Mizeraczyk<sup>b</sup>, G. Touchard<sup>c</sup>

<sup>a</sup>Department of Engineering Physics, McMaster University, Hamilton, Ontario, Canada L8S 4L7

<sup>b</sup>Institute for Fluid Flow Machinery, Polish Academy of Sciences, Gdansk, Poland

<sup>c</sup>LEA, University of Poitiers, Poitiers, France

Available online 28 November 2005

## Abstract

Experimental and theoretical investigations have been conducted for the on-set of electrohydrodynamically (EHD) induced turbulence for cylinder in cross flow. The experiments were conducted for Reynolds numbers from 0.2 to 80 based on cylinder diameters, and Reynolds numbers from  $10^3$  to  $4 \times 10^3$  based on the flow channel width. This flow conditions represent laminar to transitional-flow before the on-set of the EHD-turbulent flow. Theoretical analysis was based on the mass, momentum, and charged particle conservation equations coupled with the Poisson's equation for electric field evaluation. The results showed that: (1) on-set of EHD turbulence is initiated near the real-stagnation point; (2) EHD turbulence can be generated even for Reynolds numbers ( $Re$ ) less than 0.2, if the EHD number ( $Ehd$ ) is larger than the critical Reynolds number square ( $Ehd > Re^2$ ); and (3) the electrical origin of instability, which is leading into the on-set of turbulence can be estimated from  $Ehd/Db^2 > Re^2$  relation, where  $Db$  is the Debye number.

© 2005 Elsevier B.V. All rights reserved.

**Keywords:** Electrohydrodynamics; Corona; Turbulence

## 1. Introduction

Based on the previous experimental and theoretical work of cylinder in cross flow [1–3], flow profiles have been determined and correlated to the magnitude of the Reynolds number ( $Re_{cd} = U_o L / \nu_f$ ), where  $U_o$  is the mean velocity far upstream of the cylinder,  $L$  is the characteristic dimension either the cylinder diameter or channel width, and  $\nu_f$  is the kinematic viscosity of fluid. The results show that the flow past cylinder can be categorized in six regimes as follows: (a) For a very small Reynolds numbers ( $Re < 0.1$ ), symmetrical flow resembling non-viscous fluid flow has been observed; (b) for Reynolds numbers in the range from 0.1 to 7 ( $0.1 < Re < 7$ ), the streamlines are not symmetrical before or after the cylinder; (c) for  $7 < Re < 80$ , the recirculation wake appears in a downstream region in

the form of two symmetrical vortices; (d) for  $80 < Re < 300$ , the flow becomes unstable and laminar; (e) for larger Reynolds numbers, the flow becomes more unstable and the well-known Von Karman vortex appears. The on-set of turbulence occurs at  $Re \geq 5 \times 10^5$ .

It is well known that a space charge gradient coupled with an electric field induces instabilities leading to a fluid motion [4–7]. When the fluid is a gas, it has been observed, both theoretically and experimentally [8–10] that the electrical charges generated by corona discharge together with the electric field will generate motion of the gas, known as electrohydrodynamically (EHD) induced secondary flow or ionic wind. This type of flow can be used not only for pressure drop control in a flow channel but also for the enhancement of mass and heat transfer. Under these EHD flow, transition from laminar to turbulent flow onsets when the space charge injection exceeds the threshold value. In this paper, experimental and theoretical investigations were conducted to study the mechanisms of

\*Corresponding author. Fax: +1 905 527 5222.

E-mail address: [changj@mcmaster.ca](mailto:changj@mcmaster.ca) (J.S. Chang).

the on-set of EHD laminar to turbulent motion for cylinder and smooth wire in cross-flow.

## 2. Experimental apparatus

The first experimental flow channel for a cylinder in a cross-flow is shown in Fig. 1a. The channel was constructed from a vertical rectangular Plexiglass [11]. The cylinder, schematically shown in Fig. 1b, is placed perpendicular to the flow in the region of fully developed parallel flow. Two electrodes were mounted on the surface of the cylinder. The high voltage needle-type electrode, was placed at the front stagnation point in the median plane of the channel. The grounded electrode, was made from a flexible metal sheet placed in the rear part of the cylinder. Negative corona was generated by applying negative dc electrical potential between the needle and the grounded electrodes. The regularity of the flow is ensured by an electric fan blowing through an injector and two cellular regulators. In order to visualize the flow, a smoke generator was used to generate particles. A luminous plane for visualization is obtained by a laser, an optical fiber, and a planar lens. The flow has been recorded with a video and photo camera. All the experiments were carefully conducted under the following conditions: (a) stable upstream flow, (b) stable particle proportion, and (c) stable and uniform temperatures.

The second experimental set-up for the cylindrical wire-plate electrode system is shown in Fig. 2. A smooth corona discharge wire of 0.9 mm diameter was placed in the Plexiglas horizontal rectangular chamber. Two grounded parallel plate electrodes (20 × 60 cm) spaced by 10 cm were used as top and bottom walls of the channel. The particle image velocimetry (PIV) system as shown in Fig. 2 was the same as used by Mizeraczyk et al. [12]. TiO<sub>2</sub> powder (particle size diameter  $d_p \approx 0.2 \mu\text{m}$ ) or cigarette smoke ( $d_p < 1 \mu\text{m}$ ) was used as seed particles for a flow visualization. The experiments were conducted for flow velocities

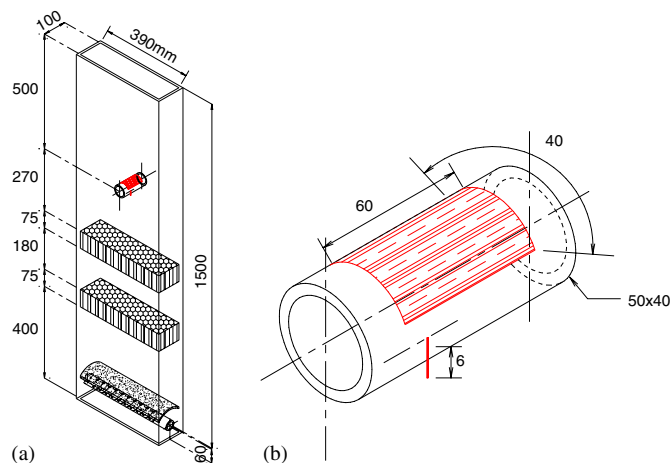


Fig. 1. Schematic of (a) experimental flow channel, and (b) details of cylindrical and electrodes arrangements.

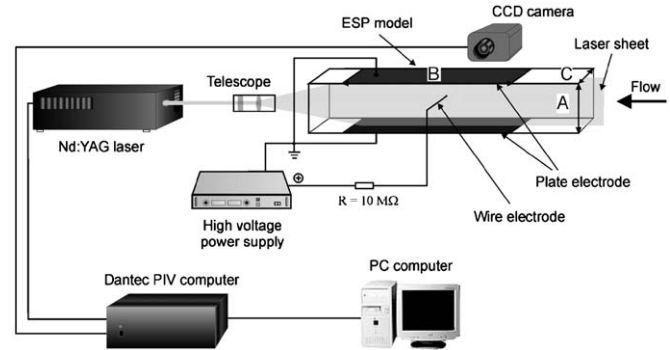


Fig. 2. Schematic of PIV system used in wide wire-plate geometry set-up. (Flow channel dimensions are as follows: plate-to-plate distance  $A = 10$  cm, plate length  $B = 60$  cm, and plate width  $C = 20$  cm).

from 0 to 0.6 m/s at positive and negative applied voltages ranging in magnitude from 0 to 30 kV.

## 3. Experimental results

Experimentally observed quasi-steady state flow pattern at  $Re = 35$  is shown in Fig. 3 for various applied voltages. Since current flows along the cylinder surface and current flux density diverged from needle electrode to plate electrode, the flow recirculation will be generated first near the needle electrode [4]. The size of EHD recirculation flow increases with increasing current flow and finally integrates with the flow wake. The directions of EHD flow streamline opposes direction of recirculation and flow wake, thus the size of the wake reduces and deforms with increasing voltage. At the same time, the current flux density near the grounded electrode increases, and hence small recirculation EHD flow will be generated near stagnation point that will deform the flow wakes. When applied voltage or discharge current is above certain threshold value, the flow is no longer steady-state and the transition to unsteady flow occurs, leading into turbulent flow.

Based on the dimensionless analyses of the Navier–Stokes Equation [6,13], the EHD secondary flow becomes significant when

$$\text{Ehd}/Re^2 \geq 1, \quad (1)$$

where  $Re = U_\infty L / \nu_f$ ,  $\text{Ehd} = I_s L^3 / A \rho \nu_f^2 \mu_i$ ,  $L$  is the diameter of cylinder,  $U_\infty$  is the gas flow,  $\nu$  is the kinematic viscosity,  $I_s$  is the total current,  $A$  is the electrode surface area,  $\rho$  is the gas density,  $\mu_i$  is the mobility of ions. Time averaged current–voltage characteristics observed from experiments is shown in Fig. 4 for various Reynolds numbers. Hence, predicted transition line (shown by dashed line in Fig. 4) can be calculated based on (1) with the following parameters:  $\mu_i = 2 \text{ cm}^2/\text{V s}$ ;  $\rho = 1.2 \text{ kg/m}^3$ ;  $A = 40 \times 60 \text{ mm}$ ;  $L = 50 \text{ mm}$ ; and  $\nu_f = 1.52 \times 10^{-5} \text{ m}^2/\text{s}$ .

If we considered the total time-averaged current, hence  $\text{Ehd}/Re^2$  as a parameter, critical EHD flow onset can be observed near 3.5 kV. A formation of forward wake (flow recirculation upstream of cylinder) can be observed as

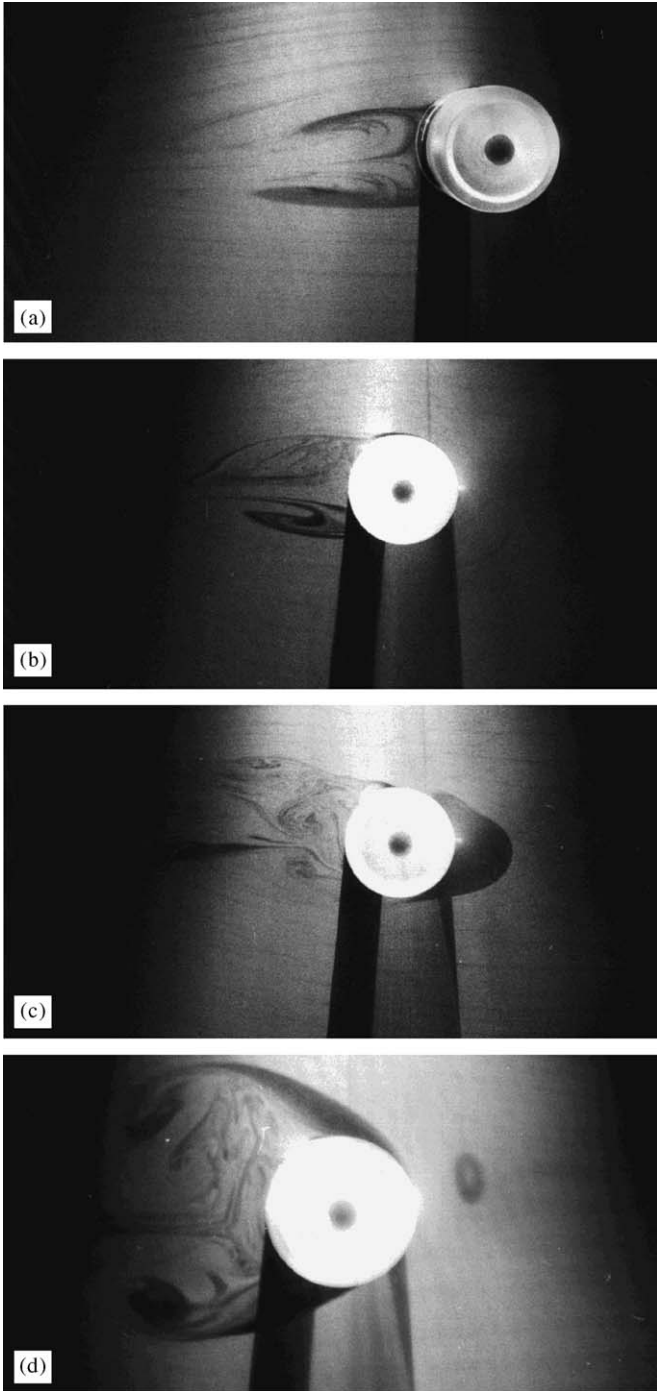


Fig. 3. Typical flow patterns for cylinder in a cross-flow geometry observed for various applied voltages: (a)  $Re = 35$ ;  $V = 0$  (kV), (b)  $Re = 35$ ;  $V = 4.5$  (kV), and (c)  $Re = 35$ ;  $V = 5$  (kV).

predicted by  $Ehd \approx Re^2$  condition. Typical current–voltage characteristics as shown in Fig. 4 for  $Re = 35$  indicated that  $Ehd = Re^2$  is fulfilled at 7 kV range. If we considered peak pulse current instead of time-averaged one, since corona discharge is normally a multiple pulse corona current,  $Ehd \approx Re^2$  accurately predicts the on-set of forward wakes.

Fig. 5 shows a typical PIV images of wire-plate system observed at various applied voltages for Reynolds number

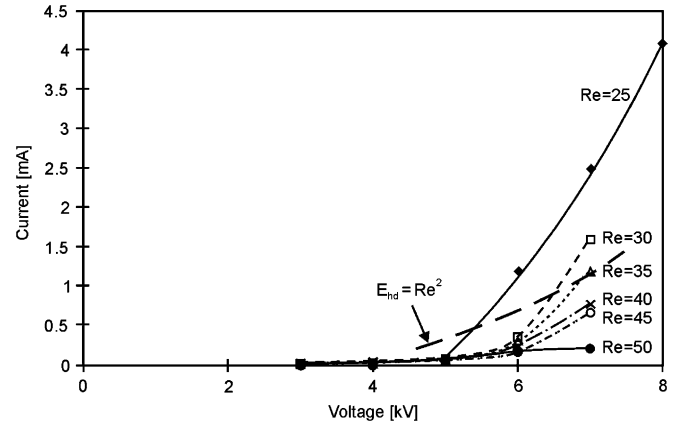


Fig. 4. Time-averaged current–voltage characteristics.

based on wire diameter of  $Re_w = 28$  and Reynolds number based on the flow channel width of  $Re_d = 2800$ . Without an applied voltage  $V = 0$  (kV) for which the  $Ehd$  number based on the wire and channel are  $Ehd_w = 0$  and  $Ehd_d = 0$ , respectively, Fig. 5 shows laminar flow in the channel and near the wire, where the wake behind the wire is so small to be observed by PIV images.

However, once  $Ehd$  numbers have been increased to  $Ehd_w = 2.3 \times 10^6$  ( $Ehd_d = 8.4 \times 10^6$ ) and  $Ehd_w = 5.7 \times 10^6$  ( $Ehd_d = 2.1 \times 10^7$ ), as shown in Figs. 5b and c, respectively, not only unsteady wakes observed but also some forward wakes were evident. The EHD-induced von-Karman vortex stream shown in Fig. 6 was usually observed before onset of turbulence observed around  $Ehd_w = 5\text{--}8 \times 10^5$ . The on-set of turbulence in relation to  $Re$  and  $Ehd_w$  is more clearly observed in Fig. 7, where based on the Reynolds number the flow is in a non-wake condition ( $Re_w = 5.6$  and  $Re_d = 560$ ) but  $Ehd_w = 2.3 \times 10^6$  indicates strong EHD secondary flow ( $Ehd_d = 8.4 \times 10^6$ ). The time-averaged flow streamlines (averaged over the period of 5 s) show fully developed vortex field in the entire flow channel.

#### 4. Theoretical analysis

Based on the model proposed by Chang and Watson [5], the laminar EHD flow can be analyzed by the following dimensionless conservation and transport equations:

- (i) Mass conservation

$$\nabla \cdot (\underline{u}) = 0. \tag{2}$$

- (ii) Momentum conservation

$$\frac{\partial \underline{u}}{\partial \tau} + \underline{u} \cdot \tilde{\nabla} \underline{u} = -\tilde{\nabla} p + \frac{Ehd}{Re^2} n_i \underline{\eta} + \frac{1}{Re} \tilde{\nabla}^2 \underline{u}. \tag{3}$$

- (iii) Ion transport

$$\frac{Re Sc_i}{2} \underline{u} \cdot \tilde{\nabla} n_i + F_E \tilde{\nabla} \cdot (n_i \underline{\eta}) - \tilde{\nabla}^2 n_i = 0. \tag{4}$$

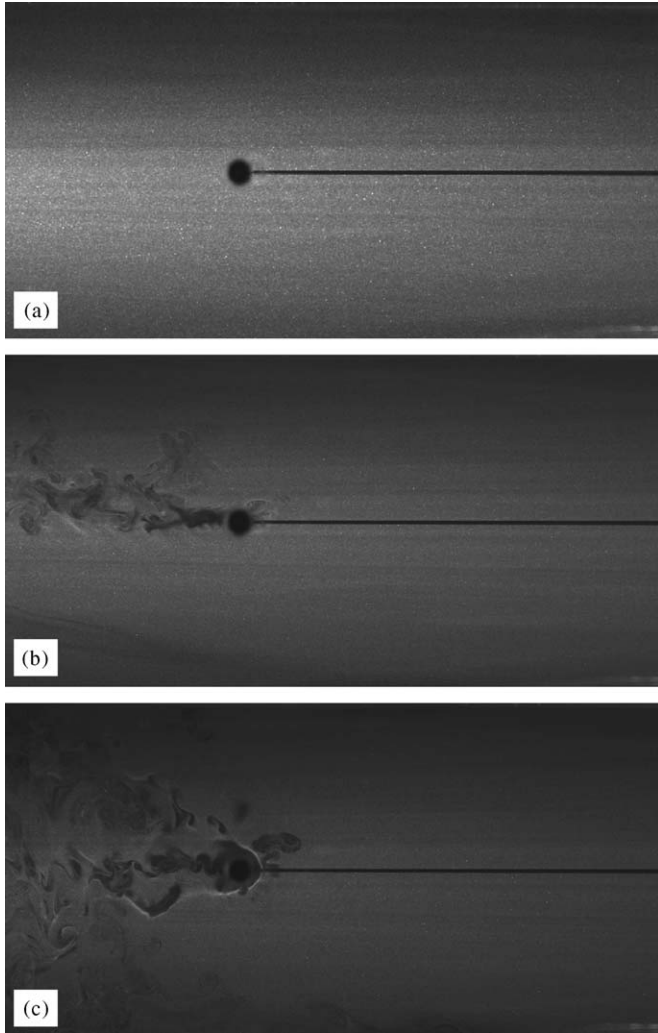


Fig. 5. Typical PIV images for wire-plate geometry at various applied voltages: (a)  $V = 0$  (kV);  $Re_w = 28$ ;  $Ehd_w = 0$ ;  $Re_d = 2800$ ;  $Ehd_d = 0$ , (b)  $V = -24$  kV;  $Re_w = 28$ ;  $Ehd_w = 2.3 \times 10^6$ ;  $Re_d = 2800$ ;  $Ehd_d = 8.4 \times 10^6$ , and (c)  $V = -30$  kV;  $Re_w = 28$ ;  $Ehd_w = 5.7 \times 10^6$ ;  $Re_d = 2800$ ;  $Ehd_d = 2.1 \times 10^7$ .

(iv) Poisson's equation

$$F_E \tilde{\nabla} \underline{\eta} = Db_i n_i. \quad (5)$$

where  $Sc_i$  is the ion Schmidt number,  $F_E$  is the electric field number,  $Db_i$  is the Debye number ( $L/8_D$ ),  $\underline{u}$  is the dimensionless velocity vector.  $8_D$  is the Debye length,  $\underline{\eta}$  is the dimensionless electric field, and  $n_i$  is the dimensionless ion density. For laminar flow,  $Ehd \geq Re^2$  is the condition when EHD flow becomes dominant. For example, the flow near cylinder was dominated by EHD flow since  $[Ehd/Re^2]_w \gg 1$  as shown in Figs. 5–7. It can be also seen that the EHD flow is not significant near the wall of the flow channel for the cases when  $[Ehd/Re^2]_d < 1$ . Hence, the onset of the turbulence can be observed when  $Ehd > Re_c^2$ , where the critical Reynolds number ( $Re_c$ ) for the on-set of turbulence are approximately  $2 \times 10^5$  and 2300 based on the cylinder and flow channel dimensions, respectively.

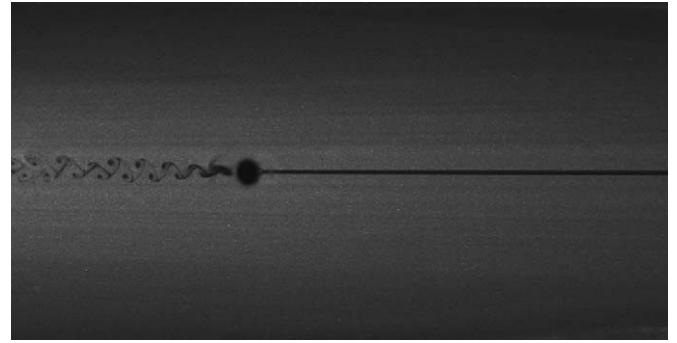


Fig. 6. EHD Von-Karman vortex at  $Re_w = 22.4$ ;  $Ehd_w = 8 \times 10^5$ ;  $Re_d = 2240$ ;  $Ehd_d = 3.1 \times 10^6$ .

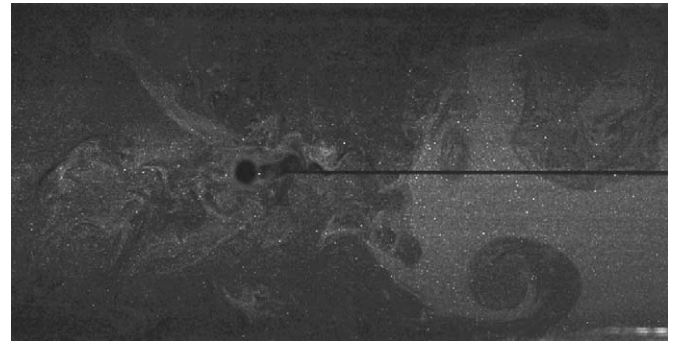


Fig. 7. Fully developed vortex at  $Re_w = 5.6$ ;  $Ehd_w = 2.3 \times 10^6$ ;  $Re_d = 560$ ;  $Ehd_d = 8.4 \times 10^6$ .

The electrical origin of the flow instability leading into onset of turbulence can be estimated from combination of Eqs. (3) and (4) for the condition of  $Ehd/Db^2 > Re^2$  for which the space charge generated electric field becomes unstable.

## 5. Concluding remarks

Based on simple charge injection-induced EHD flow model and experimental observations, we concluded that:

1. No significant flow modifications will be observed when EHD number  $Ehd \ll Re^2$ .
2. Forward wake is observed when  $Ehd \approx Re^2$  due to the charge injection (EHD flow).
3. Small recirculation will be generated along the surface of cylinder from front to real stagnation point.
4. Flow wake deformation is observed when  $Ehd \approx Re^2$ .
5. Fully developed EHD wakes are observed when  $Ehd \gg Re^2$ .
6. On-set of vortex stream tails normally observed at  $Re > 80$  can be generated even at lower Reynolds number when  $Ehd > Re^2$ .
7. On-set of EHD turbulence is usually initiated downstream of the near real-stagnation point.
8. EHD turbulence can be generated even when Reynolds numbers based on the cylinder diameter are less than 0.2, if the Ehd number is larger than Reynolds number square ( $Ehd > Re^2$ ) and the local Reynolds number

based on velocity maximum exceeds critical Reynolds number based on flow channel ( $Re_c \gg 2300$ ), and

9. The electrical origin of instability leading to the on-set of turbulence can be estimated from  $Ehd/Db^2 > Re^2$  relation.

### Acknowledgment

The authors wish to thank H. Romat, E. Moreu, G. Artana, P. Atten and C. Noger for valuable discussions and comments. This project was supported by research grant from the Region of Pictou, France, (JSC, KU, GT) and by the Polish Academy of Sciences (JM, JSC, JP, DB), and Natural Sciences and Engineering Research Council of Canada (JSC, DB, KU).

### References

- [1] M. Coutanceau, R. Bouard, *J. Fluid Mech.* 79 (1977) 231–272.
- [2] S. Taneda, *J. Phys. Soc. Japan* 14 (1959) 843–848.
- [3] C.L. Lin, S.L. Lee, *Int. J. Compounds Fluid Dyn.* 1 (1973) 235–250.
- [4] P. Atten, Electrohydrodynamic instability and motion induced by injected space charges in insulating liquids, *IEEE Trans. Dielect. Elect. Insul.* 3 (1996) 1–17.
- [5] A. Castellanos, Coulomb driven convection in electrohydrodynamics, *IEEE Trans. Elect. Inst. IE* 26 (1991) 1091–1098.
- [6] J.S. Chang, A. Watson, Electromagnetic hydrodynamics, *IEEE Trans. Dielect. Elect. Insul.* 1 (1994) 871–895.
- [7] M. Haidra, P. Atten, *IEEE Trans. Ind. Appl. Soc.* 21 (1985) 709–714.
- [8] T. Yamamoto, H.R. Velkoff, Electrohydrodynamics in electrostatic precipitator, *J. Fluid Mech.* 105 (1981) 1–18.
- [9] A. Yabe, Y. Mori, K. Hijikata, EHD study of the corona wire heating on the downstream ozone concentration profiles in an air cleaning electrostatic precipitator, *IEEE Trans. Ind. Appl. Soc.* 26 (1990) 542–549.
- [10] T. Ohkubo, S. Hamasaki, Y. Nomoto, J.S. Chang, T. Adachi, The effect of corona wire heating on downstream ozone concentration profiles in an air cleaning electrostatic precipitator, *IEEE Trans. Ind. Appl. Soc.* 26 (1990) 542–549.
- [11] C. Noger, G. Touchard, J.S. Chang, Active control of cylinder in cross flow by corona discharge induced EHD secondary flow, *Proc. ISNTP-2* (1997) 136–141.
- [12] J. Mizeraczyk, M. Kocik, J. Dekowski, M. Dors, J. Podlinski, T. Ohkubo, S. Kanazawa, T. Kawasaki, *J. Electrostat.* 51–52 (2001) 272–278.
- [13] IEEE-DEIS-EHD Technical Committee, Dimensionless parameters for EHD flow, *IEEE Trans. DEI* 10 (2003) 3–6.